

Estimating Cosmological Parameters and Reconstructing Hubble Constant with Artificial Neural Networks: A Test with Reconstructed $H(z)$

Jie-feng Chen^{a,b,c} Tingting Zhang^d Tong-Jie Zhang^{c,1,2} Ning Gai^{a,e,3}

^aCollege of Physics and Electronic information, Dezhou University,
Dezhou 253023, China

^bDepartment of Physics, Autonomous University of Barcelona,
Barcelona, 08193, Spain

^cDepartment of Astronomy, Beijing Normal University,
Beijing 100875, China

^dCollege of Command and Control Engineering, PLA Army Engineering University,
Nanjing 210000, China

^eInternational Centre of Supernovae (ICESUN), Yunnan Key Laboratory,
Kunming 650216, China

E-mail: 101101964@seu.edu.cn, tjzhang@bnu.edu.cn, gaining@dzu.edu.cn

Abstract. In this work, we present a new approach to constrain the cosmological parameters and estimate Hubble constant. We reconstructed a function from observational Hubble data using an Artificial Neural Network (ANN). The training data we used are covariance matrix and mock $H(z)$. With the reconstructed $H(z)$, we can get the Hubble constant, and thus do the comparison with the CMB-based measurements. Furthermore, in order to constrain the cosmological parameters, we sampled data points from the reconstructed data and estimated the posterior distribution. The constraining result behaved well comparing to the ones from the mock observational Hubble data. We propose that the $H(z)$ reconstructed by our artificial neural network can represent the actual distribution of real observational data, and therefore can be used in further cosmological research.

¹Also at Beijing Normal University.

²Corresponding author.

³Also at Dezhou University.

Contents

1	Introduction	1
2	Methodology	2
2.1	Neural Network	2
2.1.1	Layers	2
2.1.2	Activation functions	3
2.1.3	Back propagation, learning rate and Loss functions	3
2.1.4	Convolutional neural network	5
2.1.5	Batch Size	6
2.2	The Artificial Neural Networks in This Work	6
3	data	7
3.1	The Real OHD We Used in the Work	7
3.2	The Mock OHD	7
3.3	The covariance matrix	10
3.3.1	The Gaussian Process regression	10
3.3.2	GPR with the python package scikit-learn	12
3.3.3	The generation of the covariance matrix	13
4	Reconstruction and Parameter limitations	14
4.1	MCMC method	14
4.2	Reconstruction of $H(z)$	15
4.3	The Hubble constant from the reconstructed $H(z)$	15
4.4	Estimation with reconstructed $H(z)$	16
4.5	Estimation with Mock $H(z)$	17
5	conclusions and Discussions	17
5.1	Conclusions	17
5.2	Discussions	19

1 Introduction

The accelerating expansion of the universe is one of the most important discoveries in modern cosmology research. For the purpose to explain the accelerating expansion phenomenon, constraining cosmological parameters and estimating Hubble constant have long been basic tasks in cosmology.

There are many different kinds of data in the existing observational datasets, e.g. Damped Lyman - α Absorber (DLA) of HI 21 cm system [33, 34], observational Hubble parameter data (OHD, Jesus *et al.* [26]), type Ia supernovae (SNe Ia, [55]), cosmic microwave background ([55]), and large-scale structures [47]. Besides constraining the cosmological parameters [44, 74], with the observational data, we can understand the neutrino condensation [72], searching for extraterrestrial intelligence [35, 60] and so forth. However, in some occasions, because of the insufficiency of the existing data, we need to reconstruct or interpolate the observational data, according to the real observational datas and hypotheses.

At the same time, in the past few decades, the artificial neural networks (ANN) developed rapidly [67]. The introduction of deep learning architectures enabled training of very deep neural networks with numerous layers. Deep learning models like Transformer networks, GANs (Generative Adversarial Networks, [20]), and BERT (Bidirectional Encoder Representations from Transformers [29]) have demonstrated remarkable performance in different applications. Therefore, more and more astrophysics tasks started to apply ANNs, such as processing large scale astronomical data [8], constraining the cosmological parameters [10, 64] and data reconstruction [75].

Our work aims to constrain cosmological parameters and estimate Hubble constant with reconstructed $H(z)$ based on the OHD, so the first step is reconstruction. Before then, many people tried to perform reconstruction or interpolation tasks with artificial neural network in the cosmology, for instance, [63] reconstructed the Hubble parameter, [32] reconstructed the distance modulus and [43] reconstructed the dark energy scalar field potential. In this work, we attempt to reconstruct the Hubble parameter in the redshift range of $z \in [0, 2]$. We proposed a new method to complete reconstruction in our work, combining the mock data and the covariance matrix.

This paper is organized as follows: In section 2, firstly we briefly introduce the basic knowledge of the neural network, and how we realize the reconstruction with ANN. In section 3, we introduce the OHD data we use in this project. Besides, we also show the reason why we added an additional covariance matrix to the neural network, and how we built it. Meanwhile, we briefly introduce the Gaussian process Regression, which is the method of generating the covariance matrix. In section 4, we show the reconstructed Hubble data generated by the neural network, and we calculate the Hubble constant [18, 25] with the reconstructed data. Meanwhile, in order to constrain the cosmological parameters, we sampled datapoints from the reconstructed data and calculated the posterior distribution. In order to test the quality, we calculated the distributions with the reconstructed data and the real observational data respectively, and then compared the two results. Furthermore, we briefly introduce MCMC method, by which we constrained the cosmological parameters. Finally in Section 5, we will discuss our work and conclude.

2 Methodology

In the first few subsections of this section, we will briefly introduce the basic structure of the artificial neural networks, and finally we will show how we build our own neural network to realize the reconstruction.

2.1 Neural Network

ANN(Artificial Neural Network, or Neural Network) [70] is a mathematical model which is inspired by the structure and functions of biological neural network. The main purpose of an ANN is to construct an approximate function which can associate the input data with the output data.

2.1.1 Layers

Neural networks are typically divided into input layers, hidden layers, and output layers. The input layer receives external information (the input data), the output layer produces the final result (the output data), and the intermediate hidden layer is responsible for some complex

information processing. The input values will be processed by the layers successively. A basic structure showed as 1.

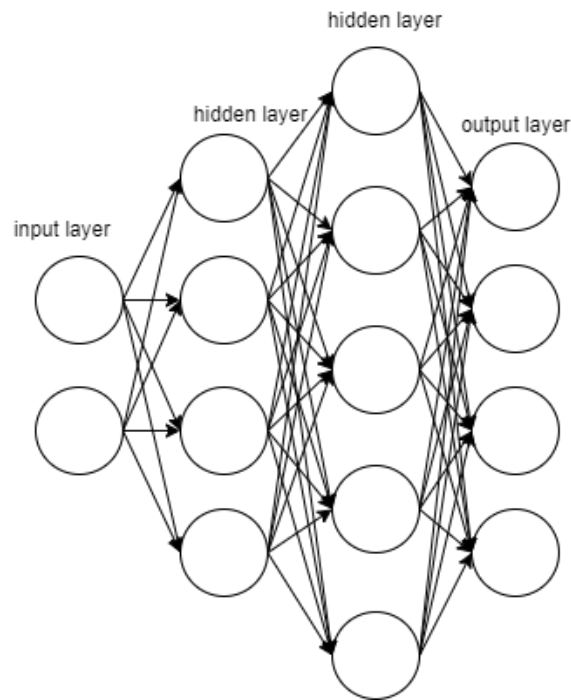


Figure 1. This is a basic structure of a ANN. There are input layer, hidden layer, hidden layer and output layer. As it should be, the neural network in practical will be more complicated.

2.1.2 Activation functions

The activation function [51] is mainly used to improve the expressive power of neural networks, enabling them to learn more complex nonlinear patterns. In neural networks, each neuron has an activation function to process the received input signal and obtain a specific output. In the neural network, the most common used activation functions are Sigmoid [30], ReLU [11], Tanh [16], etc. Shown as fig. 2, the activation function functions when the values transfers between units, or more precisely, between layers. For example, when we get a new value with a unit by the function:

$$h = \omega_1 x + b, \quad (2.1)$$

we can add an activation function so that we can get a non-linear result:

$$h = f(\omega_1 x + b), \quad (2.2)$$

Therefore, we can make the network more flexible.

2.1.3 Back propagation, learning rate and Loss functions

As we can see from the 2.1.1, the values in a neural network are propagated forward [59], from the input layer to the output layer. However, there is also a back propagation [22] while training the neural network.

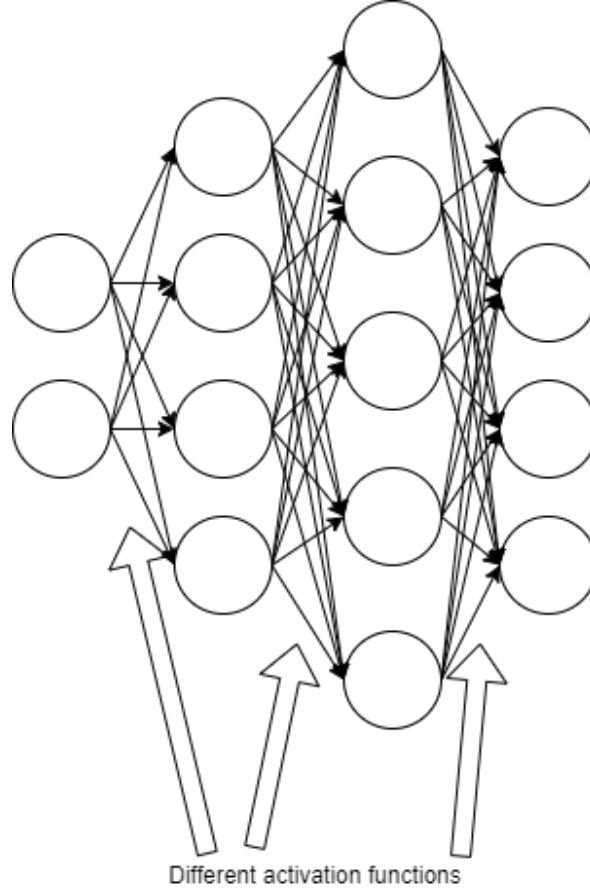


Figure 2. From the figure, we can see that the activation functions function between 2 units, which are conneced in 2 adjacent different layers.

Fig. 3 shows how back propagation and loss function work. In the first step, it calculates the loss between the output data and the target with loss function. For example, the Mean Squared Error Loss [65] is widely used in neural networks:

$$L = \frac{1}{N} \sum_{i=1}^N (y_i - \hat{y}_i)^2. \quad (2.3)$$

Having the loss, we can calculate the gradient with the equation:

$$x = x - \eta \frac{\partial L}{\partial x}, \quad (2.4)$$

where x means the weight or bais of a random unit (seen in the eq. 2.2), and η means the learning rate. As for the learning rate, as we can see from the eq. 2.4, the learning rate controls the update of the neural network. Therefore, it is important to choose an appropriate learning rate [21] in the begining of the training and adjust the learning rate when the loss is unable to converge. Thus, with the previous steps, the whole neural network update the units with the back propagation layers by layers.

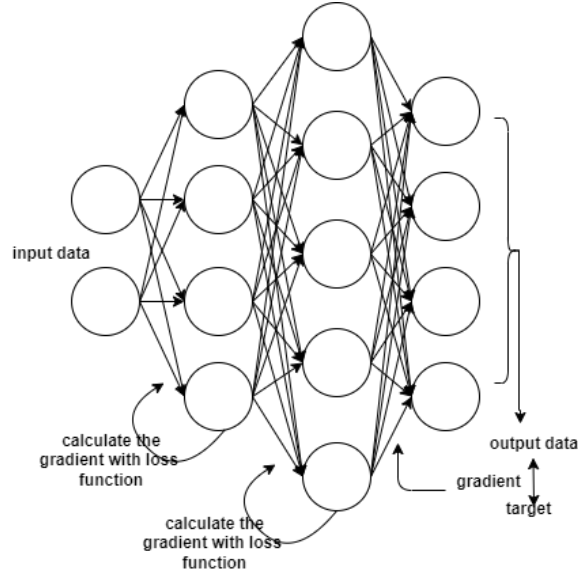


Figure 3. In the back propagation, the first step is to calculate the loss between the output data and target, and thus calculate the gradient of the output layer. Then with the same method, we calculate the loss and the gradient of the layer before the output layer. Following the same operation, we can update all the unit with the eq. 2.4 layers by layers until the input layer.

2.1.4 Convolutional neural network

In our work we used a special neural network called the convolutional neural network (CNN) [69], so in this subsection we briefly introduce CNN.

CNN is widely used in the image processing [3, 68], language analysis [23] and sound processing [49, 53]. One of the characteristic of CNN is that the dimension of the input data of the CNN is more than 1. For example, when processing the image data, the input picture will be in shape 2D. At the same time, unlike the normal neural network, CNN has many special layers, such as convolution layer, pooling layer and full connected layer. A basic structure of the CNN shown in fig. 4.

Normally, the input layer of the CNN is called the convolution layer. When training, in the beginning, the convolution layer will convert the input data into a smaller size with a kernel (or filter) [24], for example, converting the input shape (200*200) into shape (100*100). Then the pooling layer will further shrink the data and finally the full connected layer will convert the two-dimensional data into one-dimensional. However, it is noted that the principle of the convolution layer and pooling layer is different.

The convolution layer multiplies a movable small window with the two-dimensional input element by element and then adds them together [14]. This small window is actually a fixed set of weights, which can be seen as a specific filter or convolution kernel. The name "convolution" for this operation comes from the process of element level multiplication and summation. This operation is the origin of the name convolutional Neural Network. After the convolution operation, the size of the input data will be smaller.

Like the convolution layer, the pooling layer also uses a small window to shrink the two-dimensional data. Instead of calculation, the small window selects the biggest (or the mean or some parameter) value in the window, and then moves to the next element [56].

Finally, a fully connected layer realizes the process of unfolding the feature map (matrix)

obtained by convolving the last layer into a one-dimensional vector.

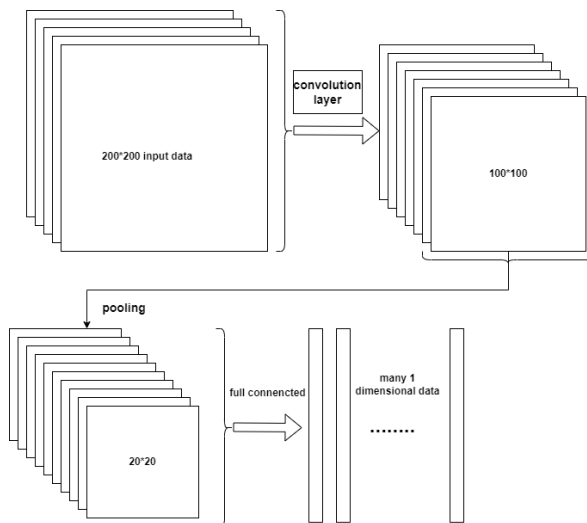


Figure 4. In this figure, we show the basic structure of the CNN. The convolution layer and pooling layer shrink the input two-dimensional data into a smaller shape with different methods. Finally the full connected layer convert the two-dimensional data into one-dimensional data.

2.1.5 Batch Size

In our work, in order to calculate the covariance matrix of the output data, we applied a we applied a relatively large batch. Batching allows for more efficient computation, especially when using GPUs. Therefore, batching in neural networks is essential. [71]

Generally, the training dataset of a neural network is divided into smaller groups called batches. Each batch contains a fixed number of training examples (batch size). For each batch, the neural network performs a forward pass, where it processes the inputs through the network layers to produce predictions. After the forward pass, the loss (a measure of how far the predictions are from the actual labels) is computed for the entire batch. The loss is typically averaged over all examples in the batch. The network then performs a backward pass to compute gradients with respect to the loss. These gradients are used to update the weights of the network. In the case of mini-batch gradient descent, these gradients are averaged over the batch. In a word, the training data pass in the network in the form of batch, instead of a single set.

2.2 The Artificial Neural Networks in This Work

In our work, we tried to reconstruct the $H(z)$ in the range of $z \in [0, 2]$. As shown in the fig. 5, in the begining of our neural network, we built a CNN to process the two-dimensional covariance matrix. After the two-dimensional input data was converted into one-dimensional, we added the z (redshift) to the network and built a full connected network. Finally, in the output part of the neural network, we got the reconstructed $H(z)$ in the range of $z \in [0, 2]$. (In shape (200,))

In our nueral network, the loss consists of two parts: the loss of the reconstruction and the loss of the covariance matrix. Firstly, we will calculatet the reconstruction loss between

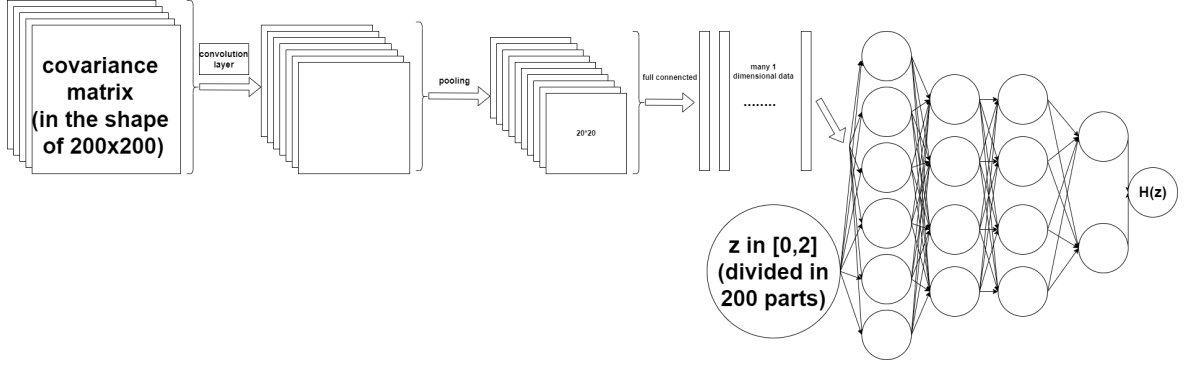


Figure 5. In this figure, we show the structure of our neural network. The network is the combination of a CNN and a full connected network. Because one of the input data is in shape (200, 200), we firstly built a CNN. In the left part, we can see that after the convolution layer, pooling layer and the full connected layer, the covariance matrix is converted into one-dimensional vector. Hence, we can input another one-dimensional input data. In the right part, we built a normal full connected network. We input two inputs, one is the redshift in the range [0, 2] and the other is the one-dimensional processed covariance matrix. Finally, the shape of the output we set is (200,), because we hope the output represents the $H(z)$ in the redshift of $z \in [0, 2]$.

the output and the training data with MSE (mean squared error) loss:

$$Loss_{reconstruction} = \frac{1}{n} \sum_{i=1}^n (H(z)_i - \hat{H}(z)_i). \quad (2.5)$$

Then we calculate the covariance matrix of the output data, and calculate the MSE with the input covariance matrix.

$$Loss_{covariance} = \frac{1}{n} \sum_{i=1}^n (cov_i - \hat{cov}_i). \quad (2.6)$$

We name it covariance loss. With the combination of two losses, we hope that the output of our neural network could learn the characteristics of the two training data.

3 data

3.1 The Real OHD We Used in the Work

The real OHD is composed of z_i , $H(z_i)$ and σ_i , where z_i is the redshift, and $H(z_i)$ is the corresponding Hubble parameter and σ_i is the corresponding uncertainty. The 32 OHD data points we used in this work are evaluated with the cosmic chronometer method, which are given in [28], [57], [58], [41], [52], [15], [40], [27] and [38], and are shown in Table. 1 and Fig. 6.

3.2 The Mock OHD

According to the flat Λ CDM model, the Hubble parameter is expressed by redshift z with the simple formula:

$$H(z) = H_0 \sqrt{\Omega_m(1+z)^3 + \Omega_\Lambda}, \quad (3.1)$$

Table 1. 32 OHD measured by the cosmic chronometer method. The OHD data is listed in time sequence. The unit of H and σ are $\text{km s}^{-1}\text{Mpc}^{-1}$

References	z	H	σ
[28]	0.09	69	12
[57]	0.17	83	8
	0.27	77	14
	0.4	95	17
	0.9	117	23
	1.3	168	17
	1.43	177	18
	1.53	140	14
	1.75	202	40
[58]	0.48	97	62
	0.88	90	40
[41]	0.1791	75	4
	0.1993	75	5
	0.3519	83	14
	0.5929	104	13
	0.6797	92	8
	0.7812	105	12
	0.8754	125	17
	1.037	154	20
[15]	0.07	69	19.6
	0.12	68.6	26.2
	0.2	72.9	29.6
	0.28	88.8	36.6
[38]	1.363	160	33.6
	1.965	186.5	50.4
[40]	0.3802	83	13.5
	0.4004	77	10.2
	0.4247	87.1	11.2
	0.4497	92.8	12.9
	0.4783	80.9	9
[52]	0.47	89	34
[27]	0.8	113.1	15.1

where the H_0 is the Hubble constant. At the same time, the Hubble parameter can also be given by the non-flat ΛCDM model:

$$H(z) = H_0 \sqrt{\Omega_m(1+z)^3 + \Omega_\Lambda + \Omega_k(1+z)^2}. \quad (3.2)$$

In our work, we generated the mock $H(z)$ with the flat ΛCDM model (According to Eq. 3.1), with the fiducial $H_0 = 67.4 \text{ km s}^{-1} \text{ Mpc}^{-1}$ and $\Omega_m = 0.314$ [1]. In the first place, we should generate the error of the mock data. With the same error method used by [36], we assumed that the error of $H(z)$ increases linearly with the redshift. We firstly fitted $\sigma_{H(z)}$ with first degree polynomials and obtain $\sigma_0 = 9.72z + 14.87$ (the red dashed line). Here we assumed that σ_0 is the mean value of $\sigma_{H(z)}$ at a specific redshift. And then, two

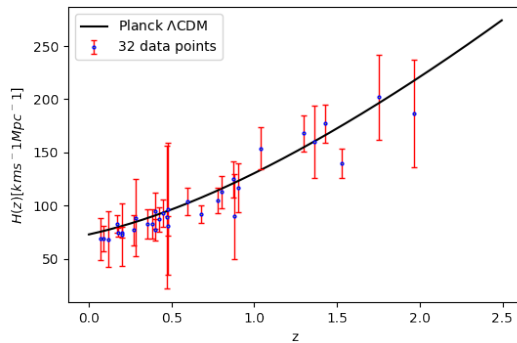


Figure 6. The 32 data points we used in this work. In order to get rid of the influence of the model, we use the data points evaluated with the model independent method. For illustrative purposes only, we include the $H(z)$ prediction assuming a Λ CDM model with Planck Collaboration [1]. In the model, the $\Omega_\Lambda = 0.686$, the $\Omega_m = 0.314$ and the $H_0 = 67.4 \text{ km s}^{-1} \text{ Mpc}^{-1}$. The curve basically fits the distribution of data points.

lines (the blue solid lines) are selected symmetrically around the mean value line to ensure that most data points are in the area between them, and these two lines have the functions of $\sigma_- = 2.92z + 4.46$ and $\sigma_+ = 16.52z + 25.28$, which are shown in the Fig. 7. Finally, the error $\sigma(z)$ was generated (or sampled) randomly according to the Gaussian distribution $\mathcal{N}(\sigma_0(z), \varepsilon(z))$, where $\varepsilon(z) = (\sigma_+ - \sigma_-)/4$ was set to ensure that $\sigma(z)$ falls in the area with a 95% probability.

The fiducial values of the Hubble parameter $H_{\text{fid}}(z)$ generated using Eq. 3.1 are simulated randomly by adding ΔH subject to $\mathcal{N}(0, \varepsilon(z))$. Thus, we can obtain the H_{moc} with the formula:

$$H_{\text{moc},i} = H_{\text{fid}}(z_i) + \Delta H_i, \quad (3.3)$$

where z_i is in the redshift range $[0, 2]$. We show the mock $H(z)$ in Fig. 8, we generated 10000 data points and plotted the 1σ , 2σ and 3σ of the distribution.

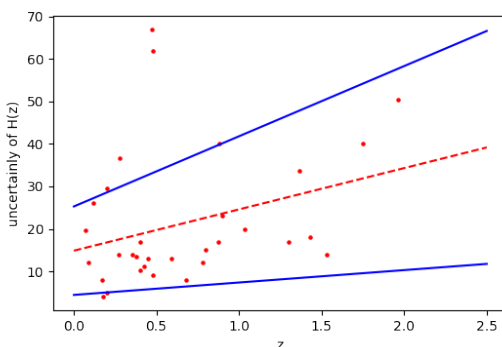


Figure 7. The error model of the mock $H(z)$ [36]. We sample the error (ΔH_i) of the mock $H(z)$ in the region between two blue lines, the redshift range of $[0, 2.5]$. The red line means the fitted equation of the distribution of the error of the observational data. In this model, we gave up the two points above, for the reason that they are too away from the other data points.

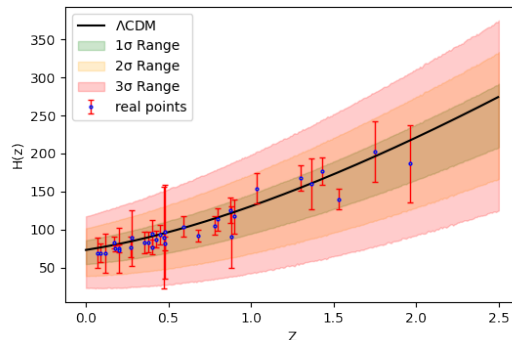


Figure 8. The 1σ , 2σ and 3σ of the mock $H(z)$. We had generated 10000 mock $H(z)$ points. In this figure, Fig. 6 and Fig. 7, we show the redshift in the range of $[0, 2.5]$, but as we can see the biggest OHD data point is actually just around 2, so in this work we just tried to reconstruct the $H(z)$ in the redshift range of $[0, 2]$.

3.3 The covariance matrix

Firstly, we will briefly introduce the Gaussian process [37], because we generate the covariance matrix based on the Gaussian process regression [66]. Then we show the method how we generate the covariance matrix.

3.3.1 The Gaussian Process regression

In theory, GPR (Gaussian process regression) is a stochastic process (a set of random variables indexed in time or space), where each set of these random variables follows a multivariate normal distribution, meaning that each finite linear combination of them follows a normal distribution. The distribution of Gaussian processes is the joint probability distribution of all the given random variables. Therefore, we can understand regression as fitting, such as linear fitting, which is fitting some data into a straight line. In practical application, GPR is the process of fitting data into Gaussian processes to achieve prediction.

For a one-dimensional Gaussian distribution, we can represent it by the mean and variance of the data:

$$x \sim N(\mu, \sigma^2), \quad (3.4)$$

$$f(x) = \frac{1}{\sigma\sqrt{2\pi}} \exp\left(-\frac{(x - \mu)^2}{2\sigma^2}\right). \quad (3.5)$$

For a two-dimensional Gaussian distribution, we can represent it by the mean of these two data points and the covariance matrix between them. Like the eq. 3.4, here $X \sim N(\mu, \Sigma)$, and Σ is the covariance matrix of the two variables, we get the distribution:

$$f(x) = \frac{1}{\sigma\sqrt{2\pi}} \exp\left(-\frac{(x - \mu)^2}{2\sigma^2}\right). \quad (3.6)$$

When it comes to the countless multidimensional Gaussian distributions over a continuous domain, we use the mean of each point and the covariance matrix between these points to represent this infinite dimensional Gaussian distribution, i.e. Gaussian process:

$$S(x_1, x_2 \dots x_n \dots) \sim N(\mu(x), \Sigma(x_i, x_j)), \quad (3.7)$$

where x_i means the i th variable, μ means the mean function and Σ means the covariance function.

When we want to do the regression operation, we can do the prediction with the equation:

$$y^{(i)} = f(x^{(i)}) + c^{(i)}, i = 1, \dots, n, \quad (3.8)$$

where $c^{(i)}$ means the noise variable, following a function $N(0, \sigma^2)$. We assume that $f(x^{(i)})$ follows a Gaussian process:

$$f(x) \sim N\left(\begin{bmatrix} m(x_1) \\ m(x_2) \\ \vdots \\ m(x_n) \end{bmatrix}, \begin{bmatrix} k(x_1, x_1) & k(x_1, x_2) & \dots & k(x_1, x_n) \\ k(x_2, x_1) & k(x_2, x_2) & \dots & k(x_2, x_n) \\ \vdots & \vdots & \ddots & \vdots \\ k(x_n, x_1) & k(x_n, x_2) & \dots & k(x_n, x_n) \end{bmatrix}\right), \quad (3.9)$$

where $m(x)$ is the mean function, and $K(x, x')$ is the covariance function, as known as the kernel function. Generally, we set the mean function to 0, because the mean function is not curial here. On the other hand, the kernel function [54], is extremely important here. The kernel function is the core of Gaussian processes, which determines the properties of Gaussian processes. The properties of Gaussian processes obtained from different kernel functions are also different. The commonly used kernel function is the Gaussian kernel function, also known as the radial basis function RBF [7]. The basic form is:

$$K(x_i, x_j) = \sigma_f^2 \exp\left(-\frac{\|x_i - x_j\|_2^2}{2l^2}\right). \quad (3.10)$$

Therefore, we can do the prediction based on the GPR. Assuming we have n data points, and their coordinates, $X(x_1, x_2, \dots, x_n)$ and $Y(y_1, y_2, \dots, y_n)$. We want to predict the Y_* according to the position coordinates of predicted points X_* . Because the $f(x)$ follows the Gaussian process, the $f(X)$ and $f(X_*)$ follow joint Gaussian distribution:

$$\begin{bmatrix} f(X) \\ f(X_*) \end{bmatrix} \sim N\left(0, \begin{bmatrix} K(X, X) & K(X, X_*) \\ K(X_*, X) & K(X_*, X_*) \end{bmatrix}\right) \quad (3.11)$$

We can obtain the probability distribution of $f(X_*)$ through Bayesian formula:

$$p(f, f_*) = N\left(\begin{bmatrix} \mu_f \\ \mu_{f_*} \end{bmatrix}, \begin{bmatrix} K & K_*^T \\ K_* & K_{**} \end{bmatrix}\right) \quad (3.12)$$

$$p(f, f_*) = p(f_*|f)p(f) \quad (3.13)$$

$$p(f|f_*) = N(\mu_{f_*} + K_*K^{-1}(f - \mu_f), K_{**} - K_*K^{-1}K_*^T). \quad (3.14)$$

If we add the noise, the above formulas will be:

$$\begin{bmatrix} Y \\ Y_* \end{bmatrix} \sim N\left(0, \begin{bmatrix} K + \sigma^2 I & K_*^T \\ K_* & K_{**} + \sigma^2 I \end{bmatrix}\right) \quad (3.15)$$

$$Y_* \sim N(\mu_*, \Sigma_*) \quad (3.16)$$

$$\mu_* = K_*(K + \sigma^2 I)^{-1} Y \quad (3.17)$$

$$\Sigma_* = K_{**} + \sigma^2 I - K_*(K + \sigma^2 I)^{-1} K_*^T. \quad (3.18)$$

Therefore, we get the $p(y|x)$ in:

$$p(y|x) = \frac{1}{\sqrt{(2\pi)^n |K + \sigma^2 I|}} \exp\left(-\frac{1}{2} y^T (K + \sigma^2 I)^{-1} y\right). \quad (3.19)$$

Usually, in GPR, we need to ensure that the constructed Gaussian process expression accurately expresses the relationship between coordinate point x and data output y . Therefore, we should find a set of hyperparameters θ which make the maximal likelihood estimation $p(y|x, \theta)$. So with the equation:

$$\log p(y|x, \theta) = -\frac{1}{2} y^T (K + \sigma^2 I)^{-1} y - \frac{1}{2} \log |K + \sigma^2 I| - \frac{n}{2} \log 2\pi, \quad (3.20)$$

we can calculate the $\theta = \text{argmax} \log p(y|x, \theta)$.

3.3.2 GPR with the python package scikit-learn

In our work, we used scikit-learn [48] to do the GPR. Scikit-learn [48] is a popular open-source machine learning library in Python, which is built on top of NumPy [46], SciPy [62], and matplotlib [61]. The kernel we used is the RBF [7] Kernel, which is a default choice widely used in GPR and suitable for modeling smooth functions.

We tried the GPR with the OHD data (table. 1), the result shown in Fig. 9. As we can see in the Fig. 9, the GPR actually can complete the task of $H(z)$ as well, but the shape of the distribution is not ideal enough. When there are many data points, the region of 95% is narrow. On the other hand, when there are less data points, we can get a larger region of 95%, such as in the redshift range of [1.75, 2]. We hope the shape of the distribution has a relatively balanced interval, like the distribution in Fig. 8.

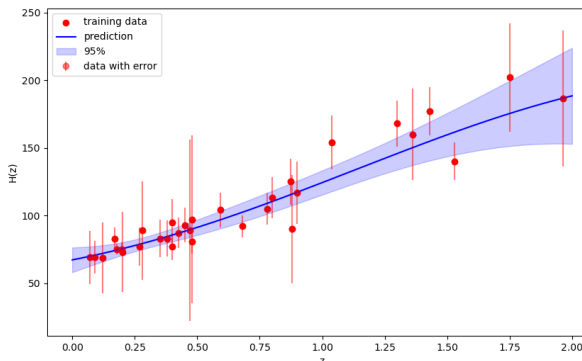


Figure 9. The reconstructed $H(z)$ with the Gaussian process regression. The shape of the distribution is not ideal enough, some part is large while the other is narrow.

3.3.3 The generation of the covariance matrix

With the $H(z)$ reconstructed with the GPR (shown in Fig. 9), we can calculate the covariance matrix, which we will use as the input data in the neural network. There are some specifically key steps of the process of calculating the covariance matrix:

(1). Sample 1000 sets of $H(z)$ in every specific redshift via the Gaussian distribution $\mathcal{N}(H(z), \sigma_{H(z)})$, where $H(z)$ and $\sigma_{H(z)}$ are the observational Hubble parameter and corresponding errors. In other word, firstly we will generate an array in shape (200, 1000) (Because we have 200 redshift in the range $z \in [0, 2]$).

(2). For two Hubble parameters at the redshift z_1 and z_2 , the covariance between them can be calculated by comparing the 1000 $H(z_1)$ and 1000 $H(z_2)$ values using the equation:

$$\text{Cov}(H(z_i), H(z_j)) = \frac{1}{N} \sum_{k=1}^N [(H(z_i)_k - \bar{H}(z_i))(H(z_j)_k - \bar{H}(z_j))], \quad (3.21)$$

where $N = 1000$, which means the number of data points at the $H(z_1)$ and $H(z_2)$, and $\bar{H}(z)$ means the average value of the 1000 $H(z)$ data points.

(3). Using the method of step 2, we can calculate the covariance between any two Hubble parameters with different redshifts. Therefore we can calculate the whole covariance matrix.

We draw the figure of the covariance matrix in Fig. 10 and randomly chose 15 data points to draw the heatmap in Fig. 12. Here we quoted the covariance matrix calculated by [39] (we show it in the Fig. 11), which represents the covariance of the $H(z)$ in the redshift region of $[0, 2]$. The covariance matrix calculated by [39] and the covariance matrix calculated with the GPR share similar characteristic: almost only having values on the diagonal line. We can clearly see that the covariance matrix of the mock $H(z)$ is consistent with the result from [39], almost only having values on the diagonal line as well.

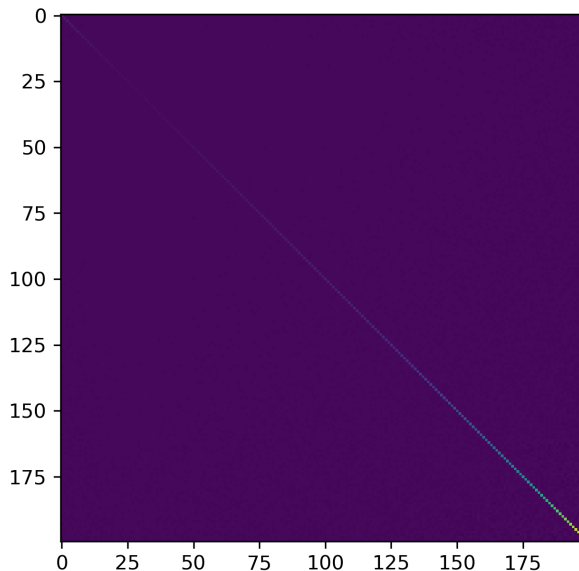


Figure 10. The full covariance matrix that generate with the $H(z)$ generated with the Gaussian process regression.

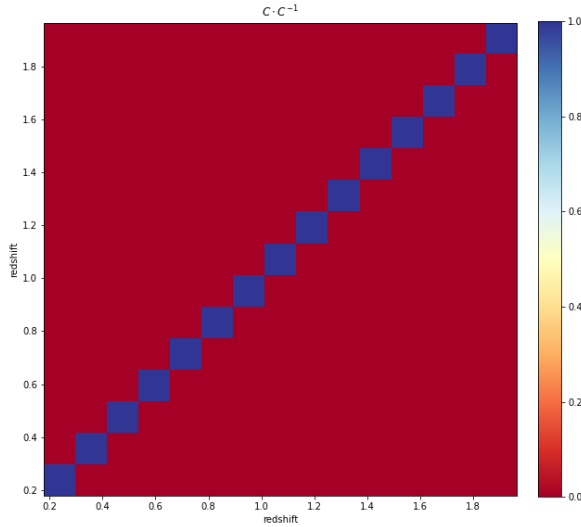


Figure 11. The covariance matrix that generate by [39]. There are only values on the diagonal line.

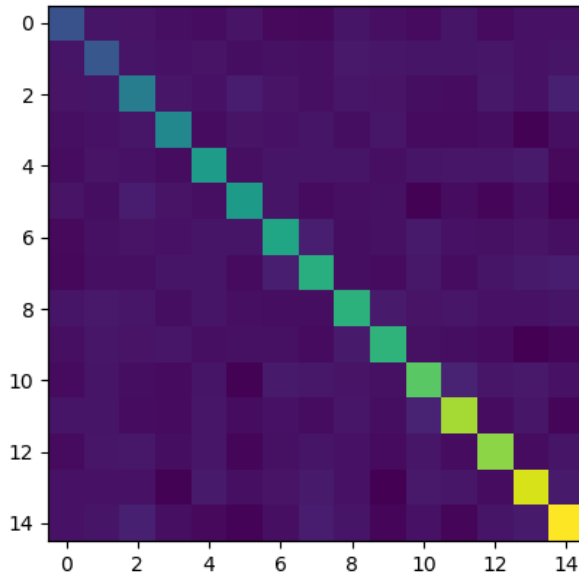


Figure 12. We took 15 data points from the $H(z)$ generated with the Gaussian process regression.

4 Reconstruction and Parameter limitations

4.1 MCMC method

Firstly, in this subsection, we briefly introduce the MCMC method (Markov chain Monte Carlo, [13, 31]), which is the method we used to calculate the posterior distribution of the cosmological parameters.

MCMC method is widely used in various fields, including Bayesian inference [73], physics, and machine learning [2]. The process of MCMC involves simulating a Markov chain [45] in the parameter space, sampling randomly and then satisfying the samples to the target probability distribution function (PDF). It proceeds as follows:

- (1). Initialization: Start from a random arbitrary initial state x_0 .
- (2). Proposal: Propose a new state x' based on a proposal distribution $Q(x'|x_t)$, which defines the probability of transitioning from state x_t to x' .
- (3). Acceptance: Calculate the acceptance probability (α) to decide whether to accept or reject the proposed state.

$$\alpha(x_t, x') = \min \left(1, \frac{P(x') * Q(x_t|x')}{P(x_t) * Q(x'|x_t)} \right) \quad (4.1)$$

If $\alpha > 1$ accept x' as the next state.

If $\alpha < 1$ accept x' with probability α and stay at x_t otherwise.

- (4). Repeat: Generate a series of states by iterating steps 2 and 3.

This process generates a sequence of states that eventually converge to samples from the target distribution $P(x)$. The samples can then be used to estimate expectations or compute integrals over the target distribution.

MCMC method has many different kinds of algorithms, such as the Metropolis-Hastings [12], which provides a way to explore complex probability distributions, allowing practitioners to draw samples from distributions that are otherwise challenging to sample directly.

The MCMC method we used in our work is Emcee [17]. Emcee is a Python package designed for running MCMC simulations. It's particularly well-suited for Bayesian inference and exploring complex, high-dimensional parameter spaces. Emcee simplifies the process of conducting MCMC simulations, making it accessible for scientists and researchers to perform Bayesian inference [6] and explore parameter spaces for various applications in statistics, machine learning, and other fields.

4.2 Reconstruction of $H(z)$

In the Fig. 13, we show the reconstruction of $H(z)$ generated with our neural network. The Fig. 13 looks like the combination of the Fig. 13 and the Fig. 9. The shape of the confidence interval of the Fig. 13 is like Fig. 9, and at the same time the interval has a more precise range comparing the Fig. 8.

4.3 The Hubble constant from the reconstructed $H(z)$

We also calculate the Hubble constant from the reconstructed $H(z)$. The Hubble constant is an important parameter in cosmology. According to the Friedman equations [19]:

$$\dot{a}^2 - \frac{1}{3}(8\pi G\rho + \Lambda)a^2 = -kc^2, \quad (4.2)$$

and

$$\frac{\ddot{a}}{a} = -\frac{4}{3}\pi G(\rho + 3\frac{p}{c^2}) + \frac{1}{3}\Lambda. \quad (4.3)$$

Here $a = a(t)$ is the scale factor of the Universe. At any given time, we can define a Hubble parameter:

$$H(t) = \frac{\dot{a}}{a}. \quad (4.4)$$

It is obvious that the Hubble constant H_0 is the value of H at the current time. In our reconstruction $H(z)$, we get the $H_0 = 68.67 \pm 5.903$. With CMB-based measurements [4, 5], it gives values of H_0 of 67-68 km s⁻¹ Mpc⁻¹ with the error of 1-2 km s⁻¹ Mpc⁻¹. The Hubble constant from our reconstructed H_0 is closed to the one from CMB-based calculation.

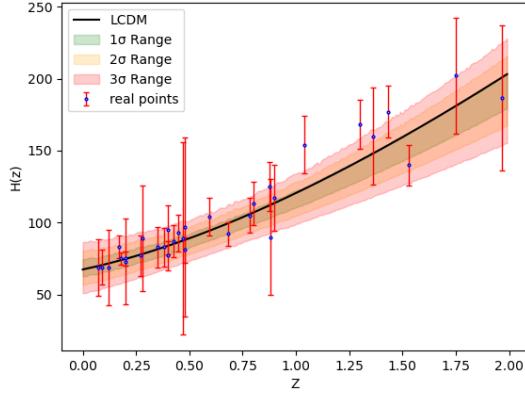


Figure 13. The 1σ , 2σ and 3σ and the reconstructed $H(z)$. This result looks decent, and is quite similar to the Fig. 8. It basically matches the Λ CDM.

4.4 Estimation with reconstructed $H(z)$

We sampled 32 data points randomly from the reconstructed $H(z)$ and applied them to constrain the cosmological parameters with MCMC method. The posterior distribution estimated by MCMC, which is shown in the Fig. 14, gives the result of $H_0 = 68.03^{+3.51}_{-3.58}$ $\text{km s}^{-1} \text{Mpc}^{-1}$, $\Omega_m = 0.27^{+0.05}_{-0.05}$, $\Omega_\Lambda = 0.73^{+0.05}_{-0.05}$.

Besides, we also calculated the posterior distribution with the real 32 OHD points in table. 1, we show the result in the fig. 15. The real 32 OHD points gives the result of $H_0 = 67.73^{+3.04}_{-3.10}$ $\text{km s}^{-1} \text{Mpc}^{-1}$, $\Omega_m = 0.33^{+0.07}_{-0.06}$, $\Omega_\Lambda = 0.73^{+0.06}_{-0.07}$.

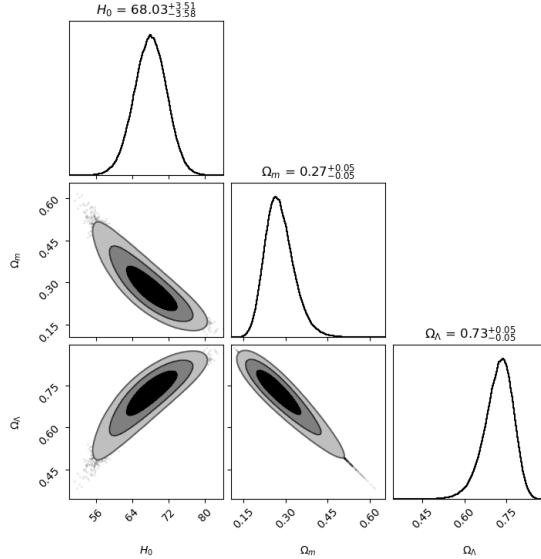


Figure 14. The posterior distribution of the random 32 points from the reconstruction $H(z)$. We calculated the posterior distribution with MCMC.

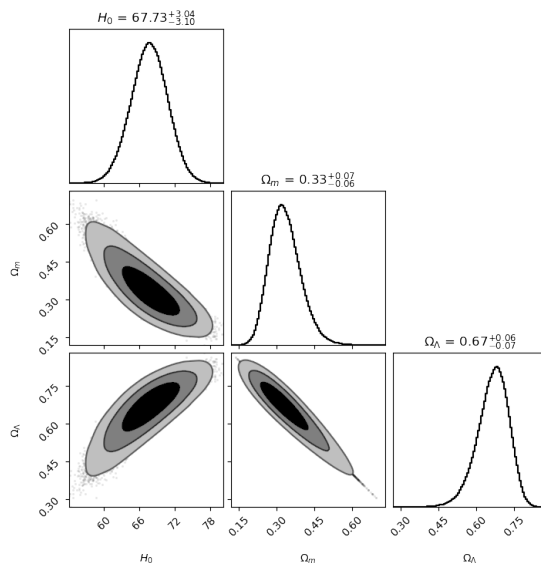


Figure 15. The posterior distribution of the 32 real data points from OHD. We calculated the posterior distribution with MCMC.

4.5 Estimation with Mock $H(z)$

At the same time, in order to do a better comparison, we also sampled 32 data points randomly from the mock $H(z)$ and applied to constrain the cosmological parameters with MCMC method. The posterior distribution estimated by MCMC, which is shown in the Fig. 16, gives the result of $H_0 = 62.04^{+15.98}_{-13.7}$ km s⁻¹ Mpc⁻¹, $\Omega_m = 0.38^{+0.30}_{-0.17}$, $\Omega_\Lambda = 0.62^{+0.17}_{-0.30}$.

It is obvious that the posterior distribution estimated with the data points from the reconstructed $H(z)$ is more closer to the roughly estimated values ($H_0 \approx 67 \text{ km s}^{-1} \text{ Mpc}^{-1}$, $\Omega_\Lambda \approx 0.7$, $\Omega_m \approx 0.3$), or more precisely, the Λ CDM model from Planck Collaboration [1], which gives the estimation of $H_0 \approx 67.4 \text{ km s}^{-1} \text{ Mpc}^{-1}$, $\Omega_\Lambda \approx 0.686$, $\Omega_m \approx 0.314$. At the same time, the confidence interval of the posterior distribution estimated with the data points from the reconstructed $H(z)$ is tighter.

5 conclusions and Discussions

5.1 Conclusions

In this work, we had put forward a new method that can be used to reconstruct the $H(z)$. The effect of this method is obvious. One of the main purposes of our work is to estimate the cosmological parameters, so we sampled some data points from the reconstructed $H(z)$ and constrained in the Λ CDM model. We found that the posterior distribution calculated by the sampled reconstructed data is consistent with the Λ CDM model with Planck Collaboration [1], behaving better than calculating the posterior distribution with the mock $H(z)$, which is one of the training data in our work. Comparing to the posterior distribution estimated with the real 32 OHD points, the result gives by the reconstructed $H(z)$ has a confidence intervals of the same size, and the 2 posterior distributions give similar range of the 3 cosmological parameters. Furthermore, the shape of the 2 distributions (Fig. 14 and Fig. 15) are similar. On the contrary, the shape and the range of the posterior distribution calculated by the mock

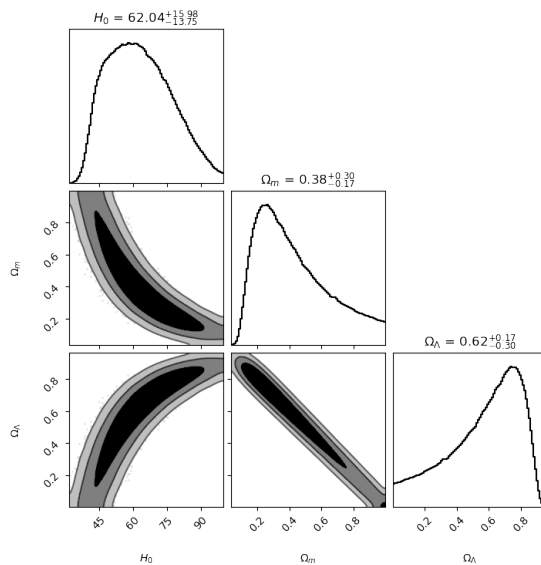


Figure 16. The posterior distribution of the random 32 points from the mock $H(z)$. We calculated the posterior distribution with MCMC.

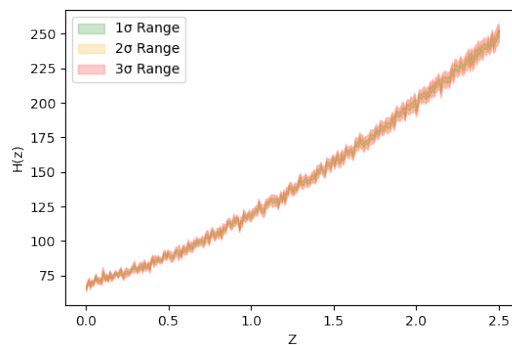


Figure 17. One "bad" posterior distribution we got when we didn't control the proportion between the covariance loss and reconstruction loss well. It is hard to see the 1σ , 2σ and 3σ , and the shape of the distribution is not smooth. In this Figure, we show the redshift of $[0, 2.5]$.

$H(z)$ didn't behave well. Apart from just sampling 32 data points, we can sample more points in the reconstructed data in the range which has few real data points. At the same time, with the reconstructed $H(z)$, we can easily get the Hubble constant H_0 , and the result is consistent with the Hubble constant calculated by the CMB-based measurements.

Therefore, we propose that the data reconstructed by our method can represent the actual distribution of the real observational data nicely, and thus can be helpful in cosmological research such as the cosmological parameter estimation and calculation of the dark energy scalar field potential. We will keep investigating these interesting issues in our future works.

We combined the real observational data and covariance matrix to generate reconstructed $H(z)$ in a specific redshift range in $z \in [0, 2]$. More precisely, we hope the reconstructed $H(z)$ can learn the characteristics of both Fig. 8 and Fig. 9. Like we talk in the 3.3.2, the shape

of Fig. 9 is not ideal enough, and as we can see the region 95% doesn't include many real data points. To some extent, it is still reasonable because when there has more data points, it is easier to get a precise estimation. On the contrary, Fig. 8 lose the precision in order to construct the balanced shape of the distribution. For this reason, in our work we decided to combine the 2 distributions in Fig. 8 and Fig. 9.

Also note that in the training process, we need to control the proportion of covariance loss in the loss function carefully. The neural network should mainly learn the properties of mock data but not the covariance matrix's. We have attempted to let the neural network primarily learn the properties of covariance matrice. As a consequence, the data points will be very discrete and hard for us to plot the 1σ , 2σ and 3σ (One of the distribution we got is the Fig. 17). Hence, we should also pay attention to find an appropriate the proportion of covariance loss and the reconstruction loss in loss function.

5.2 Discussions

Admittedly, we should pay attention to the construction of the covariance matrix we used as training data in our network, and see if we could find a better method to generate the covariance matrix. In the bigining, we tried to reconstruct the $H(z)$ in the redshif range of $[0, 2.5]$. However, when we used the GPR, the data diverged in the redshift range of $[2, 2.5]$ because of having no data points in that redshift range. Consequently, it is hard for us to calculate the covariance matrix and the posterior distribution. For this reason, we had to limite the redshift in the range of $[0, 2]$. (Fig. 17 is actually a good example here to show the importance of controlling the the proportion between the covariance loss and reconstruction loss. As we can see the redshift is in the range of $[0, 2.5]$. Although the covariance matrix was diverged, the posterior distribution still mainly learned the mock $H(z)$ but not the diverged covariance matrix.)

Besides, we should also explore the possibility of using more input data, such as the Type Ia supernovae observation data, so that we can introduce more information and reconstruct better data, and thus get better result in calculating Hubble constant and estimating cosmological parameters.

Meanwhile, ANN models usually need careful hyperparameter fine-tuning before the best performance can be achieved. Therefore, future work should be focused on finding some other better models, such as VEA-GAN [9, 42] and AVAE [50]. We hope we can find more useful models in the future work.

Acknowledgments

We thank Shiyu Li, Yunlong Li, Yu Hu, Changzhi Lu, Yuchen Wang, Shulei Cao, Jin Qin, Zhenzhao Tao, Zijian Wang, Xiaohang luan, Jing Niu, guangzai ye, zijian si and Kang Jiao for useful discussions and their kind help. This work was supported by the National SKA Program of Chinax (2022SKA0110202), China Manned Space Program through its Space Application System and National Science Foundation of China (Grants No. 61802428), China Scholarship Council (File No.202306040042) and the International Centre of Supernovae, Yunnan Key Laboratory (Nos.202302AN360001, 202302AN36000103).

References

- [1] Aghanim, N., Y. Akrami, M. Ashdown, J. Aumont, C. Baccigalupi, M. Ballardini, A. Banday, R. Barreiro, N. Bartolo, S. Basak, *et al.* (2018), arXiv preprint arXiv:1807.06209 .

- [2] Andrieu, C., N. De Freitas, A. Doucet, and M. I. Jordan (2003), *Machine learning* **50**, 5.
- [3] Anwar, S. M., M. Majid, A. Qayyum, M. Awais, M. Alnowami, and M. K. Khan (2018), *Journal of medical systems* **42**, 1.
- [4] Beutler, F., C. Blake, M. Colless, D. H. Jones, L. Staveley-Smith, L. Campbell, Q. Parker, W. Saunders, and F. Watson (2011), *Monthly Notices of the Royal Astronomical Society* **416** (4), 3017.
- [5] Blake, C., E. A. Kazin, F. Beutler, T. M. Davis, D. Parkinson, S. Brough, M. Colless, C. Contreras, W. Couch, S. Croom, *et al.* (2011), *Monthly Notices of the Royal Astronomical Society* **418** (3), 1707.
- [6] Box, G. E., and G. C. Tiao (2011), *Bayesian inference in statistical analysis* (John Wiley & Sons).
- [7] Buhmann, M. D. (2000), *Acta numerica* **9**, 1.
- [8] Cabayol-Garcia, L., M. Eriksen, A. Alarcón, A. Amara, J. Carretero, R. Casas, F. J. Castander, E. Fernández, J. García-Bellido, E. Gaztanaga, *et al.* (2020), *Monthly Notices of the Royal Astronomical Society* **491** (4), 5392.
- [9] Cemgil, T., S. Ghaisas, K. Dvijotham, S. Goyal, and P. Kohli (2020), *Advances in Neural Information Processing Systems* **33**, 15077.
- [10] Chen, J.-F., Y.-C. Wang, T. Zhang, and T.-J. Zhang (2023), *Physical Review D* **107** (6), 063517.
- [11] Chen, Y., X. Dai, M. Liu, D. Chen, L. Yuan, and Z. Liu (2020), in *European conference on computer vision* (Springer) pp. 351–367.
- [12] Chib, S., and E. Greenberg (1995), *The american statistician* **49** (4), 327.
- [13] Christensen, N., R. Meyer, L. Knox, and B. Luey (2001), *Classical and Quantum Gravity* **18** (14), 2677.
- [14] Cong, S., and Y. Zhou (2023), *Artificial Intelligence Review* **56** (3), 1905.
- [15] Cong, Z., Z. Han, Y. Shuo, L. Siqi, Z. Tong-Jie, S. Yan-Chun, *et al.* (2014), *Research in Astronomy and Astrophysics* **14**.
- [16] Fan, E. (2000), *Physics Letters A* **277** (4-5), 212.
- [17] Foreman-Mackey, D., D. W. Hogg, D. Lang, and J. Goodman (2013), *Publications of the Astronomical Society of the Pacific* **125** (925), 306.
- [18] Freedman, W. L., and B. F. Madore (2010), *Annual Review of Astronomy and Astrophysics* **48** (1), 673.
- [19] Friedman, A. (1922), *Zeitschrift für Physik* **10** (1), 377.
- [20] Goodfellow, I., J. Pouget-Abadie, M. Mirza, B. Xu, D. Warde-Farley, S. Ozair, A. Courville, and Y. Bengio (2014), *Advances in neural information processing systems* **27**.
- [21] He, F., T. Liu, and D. Tao (2019), *Advances in neural information processing systems* **32**.
- [22] Hecht-Nielsen, R. (1992), in *Neural networks for perception* (Elsevier) pp. 65–93.
- [23] Hu, B., Z. Lu, H. Li, and Q. Chen (2014), *Advances in neural information processing systems* **27**.
- [24] Huang, Q., K. Zhou, S. You, and U. Neumann (2018), in *2018 IEEE Winter Conference on Applications of Computer Vision (WACV)* (IEEE) pp. 709–718.
- [25] Jackson, N. (2015), *Living reviews in relativity* **18** (1), 2.
- [26] Jesus, J. F., T. Gregório, F. Andrade-Oliveira, R. Valentim, and C. Matos (2017), *Monthly Notices of the Royal Astronomical Society* (3), 3.

- [27] Jiao, K., N. Borghi, M. Moresco, and T.-J. Zhang (2023), *The Astrophysical Journal Supplement Series* **265** (2), 48.
- [28] Jimenez, R., L. Verde, T. Treu, and D. Stern (2003), *The Astrophysical Journal* **593** (2), 622.
- [29] Kenton, J. D. M.-W. C., and L. K. Toutanova (2019), in *Proceedings of naacL-HLT*, Vol. 1 (Minneapolis, Minnesota) p. 2.
- [30] Kyurkchiev, N., and S. Markov (2015), LAP LAMBERT Academic Publishing, Saarbrucken **4**.
- [31] Lewis, A., and S. Bridle (2002), *Physical Review D* **66** (10), 103511.
- [32] Li, S.-Y., Y.-L. Li, and T.-J. Zhang (2019), *Research in Astronomy and Astrophysics* **19** (9), 137.
- [33] Lu, C.-Z., K. Jiao, T. Zhang, T.-J. Zhang, and M. Zhu (2022), *Physics of the Dark Universe* **37**, 101088.
- [34] Lu, C.-Z., T. Zhang, and T.-J. Zhang (2022), arXiv preprint arXiv:2208.05639 .
- [35] Luan, X.-H., Z.-Z. Tao, H.-C. Zhao, B.-L. Huang, S.-Y. Li, C. Liu, H.-F. Wang, W.-F. Liu, T.-J. Zhang, V. Gajjar, *et al.* (2023), *The Astronomical Journal* **165** (3), 132.
- [36] Ma, C., and T.-J. Zhang (2011), *The Astrophysical Journal* **730** (2), 74.
- [37] MacKay, D. J., *et al.* (1998), NATO ASI series F computer and systems sciences **168**, 133.
- [38] Moresco, M. (2015), *Monthly Notices of the Royal Astronomical Society: Letters* **450** (1), L16, <https://academic.oup.com/mnrasl/article-pdf/450/1/L16/3083577/slv037.pdf> .
- [39] Moresco, M., R. Jimenez, L. Verde, A. Cimatti, and L. Pozzetti (2020), *The Astrophysical Journal* **898** (1), 82.
- [40] Moresco, M., L. Pozzetti, A. Cimatti, R. Jimenez, C. Maraston, L. Verde, D. Thomas, A. Citro, R. Tojeiro, and D. Wilkinson (2016), *Journal of Cosmology and Astroparticle Physics* **2016** (05), 014.
- [41] Moresco, M., L. Verde, L. Pozzetti, R. Jimenez, and A. Cimatti (2012), *Journal of Cosmology and Astroparticle Physics* **2012** (07), 053.
- [42] Mukesh, K., S. Ippatapu Venkata, S. Chereddy, E. Anbazhagan, and I. Oviya (2022), in *International Conference on Innovative Computing and Communications: Proceedings of ICICC 2022, Volume 1* (Springer) pp. 761–768.
- [43] Niu, J., Y. Chen, and T.-J. Zhang (2023), arXiv preprint arXiv:2305.04752 .
- [44] Niu, J., and T.-J. Zhang (2023), *Physics of the Dark Universe* **39**, 101147.
- [45] Norris, J. R. (1998), *Markov chains*, 2 (Cambridge university press).
- [46] Oliphant, T. E., *et al.* (2006), *Guide to numpy*, Vol. 1 (Trelgol Publishing USA).
- [47] Pan, S., M. Liu, J. Forero-Romero, C. G. Sabiu, Z. Li, H. Miao, and X.-D. Li (2020), *Science China Physics, Mechanics, and Astronomy* **63** (11), 110412, arXiv:1908.10590 [astro-ph.CO] .
- [48] Pedregosa, F., G. Varoquaux, A. Gramfort, V. Michel, B. Thirion, O. Grisel, M. Blondel, P. Prettenhofer, R. Weiss, V. Dubourg, *et al.* (2011), *the Journal of machine Learning research* **12**, 2825.
- [49] Piczak, K. J. (2015), in *2015 IEEE 25th international workshop on machine learning for signal processing (MLSP)* (IEEE) pp. 1–6.
- [50] Plumerault, A., H. Le Borgne, and C. Hudelot (2021), in *2020 25th International Conference on Pattern Recognition (ICPR)* (IEEE) pp. 8687–8694.
- [51] Ramachandran, P., B. Zoph, and Q. V. Le (2017), arXiv preprint arXiv:1710.05941 .

- [52] Ratsimbazafy, A., S. Loubser, S. Crawford, C. Cress, B. Bassett, R. Nichol, and P. Väisänen (2017), *Monthly Notices of the Royal Astronomical Society* **467** (3), 3239.
- [53] Salamon, J., and J. P. Bello (2017), *IEEE Signal processing letters* **24** (3), 279.
- [54] Schulz, E., M. Speekenbrink, and A. Krause (2018), *Journal of mathematical psychology* **85**, 1.
- [55] Scolnic, D. M., D. O. Jones, A. Rest, Y. C. Pan, R. Chornock, R. J. Foley, M. E. Huber, R. Kessler, G. Narayan, and A. G. Riess (2017), *Astrophysical Journal* .
- [56] Shyam, R. (2021), *Journal of Computer Technology & Applications* **12** (2), 6.
- [57] Simon, J., L. Verde, and R. Jimenez (2005), [Phys. Rev. D](#) **71**, 123001.
- [58] Stern, D., R. Jimenez, L. Verde, M. Kamionkowski, and S. A. Stanford (2009), *journal of cosmology and astroparticle physics* .
- [59] Svozil, D., V. Kvasnicka, and J. Pospichal (1997), *Chemometrics and intelligent laboratory systems* **39** (1), 43.
- [60] Tao, Z.-Z., H.-C. Zhao, T.-J. Zhang, V. Gajjar, Y. Zhu, Y.-L. Yue, H.-Y. Zhang, W.-F. Liu, S.-Y. Li, J.-C. Zhang, *et al.* (2022), *The Astronomical Journal* **164** (4), 160.
- [61] Tosi, S. (2009), *Matplotlib for Python developers* (Packt Publishing Ltd).
- [62] Virtanen, P., R. Gommers, T. E. Oliphant, M. Haberland, T. Reddy, D. Cournapeau, E. Burovski, P. Peterson, W. Weckesser, J. Bright, *et al.* (2020), *Nature methods* **17** (3), 261.
- [63] Wang, G.-J., X.-J. Ma, S.-Y. Li, and J.-Q. Xia (2020), *The Astrophysical Journal Supplement Series* **246** (1), 13.
- [64] Wang, Y. C., Y. B. Xie, T. J. Zhang, H. C. Huang, T. Zhang, and K. Liu (2021), *The Astrophysical Journal Supplement Series* **254** (2), 43 (16pp).
- [65] Wang, Z., and A. C. Bovik (2009), *IEEE signal processing magazine* **26** (1), 98.
- [66] Williams, C., and C. Rasmussen (1995), *Advances in neural information processing systems* **8**.
- [67] Wu, Y.-c., and J.-w. Feng (2018), *Wireless Personal Communications* **102**, 1645.
- [68] Xu, L., J. S. Ren, C. Liu, and J. Jia (2014), *Advances in neural information processing systems* **27**.
- [69] Yamashita, R., M. Nishio, R. K. G. Do, and K. Togashi (2018), *Insights into imaging* **9**, 611.
- [70] Yegnanarayana, B. (2009), *Artificial neural networks* (PHI Learning Pvt. Ltd.).
- [71] You, Y., I. Gitman, and B. Ginsburg (2017), arXiv preprint arXiv:1708.03888 .
- [72] Yu, H.-R., J. Emberson, D. Inman, T.-J. Zhang, U.-L. Pen, J. Harnois-Déraps, S. Yuan, H.-Y. Teng, H.-M. Zhu, X. Chen, *et al.* (2017), *Nature Astronomy* **1** (7), 0143.
- [73] Yuan, S., and T.-J. Zhang (2015), *Journal of Cosmology and Astroparticle Physics* **2015** (02), 025.
- [74] Zhang, H., Y.-C. Wang, T.-J. Zhang, and T. Zhang (2023), *The Astrophysical Journal Supplement Series* **266** (2), 27.
- [75] Zhang, J.-C., Y. Hu, K. Jiao, H.-F. Wang, Y.-B. Xie, B. Yu, L.-L. Zhao, and T.-J. Zhang (2023), arXiv preprint arXiv:2311.13938 .